Development of a Refined RTD-Based Efficiency Prediction Model for Cross-flow Trays

Vishwakarma, V.; Schubert, M.; Hampel, U.;

Originally published:

January 2019

Industrial & Engineering Chemistry Research 58(2019)8, 3258-3268

DOI: https://doi.org/10.1021/acs.iecr.8b04672

Development of a Refined RTD-based Efficiency Prediction Model for Cross-flow Trays

Journal:	*Industrial & Engineering Chemistry Research*
Manuscript ID	ie-2018-04672f
Manuscript Type:	Article
Date Submitted by the Author:	24-Sep-2018
Complete List of Authors:	Vishwakarma, Vineet; Helmholtz-Zentrum Dresden-Rossendorf; Technische Universitat Dresden Schubert, Markus; Helmholtz-Zentrum Dresden-Rossendorf Hampel, Uwe; Helmholtz-Zentrum Dresden-Rossendorf; Technische Universitat Dresden

Development of a Refined RTD-based Efficiency Prediction Model for Cross-flow Trays

Vineet Vishwakarma[a,b,*], Markus Schubert[a] , Uwe Hampel[a,b]

[a]Helmholtz-Zentrum Dresden-Rossendorf, Institute of Fluid Dynamics, Bautzner Landstraße 400, 01328 Dresden, Germany

[b]Technische Universität Dresden, AREVA Endowed Chair of Imaging Techniques in Energy and Process Engineering, 01062 Dresden, Germany

*Corresponding author: Tel.: +49 351 260 3778, Fax: +49 351 260 2383

E-mail address: v.vishwakarma@hzdr.de

Abstract: The present work describes the mathematical formulation of a new tray efficiency model through refinement of the conventional residence time distribution (RTD) approach [Foss et al., AIChE J., 1958, 4(2):231-239]. The geometrical partitioning of tray into compartments along the main liquid flow direction is a prerequisite in the new model. This partitioning allows computing the tray efficiency through quantification of the efficiency of individual compartments. The new model ensures that the fluid dynamics of each compartment contribute towards the overall tray efficiency. This breaks the previous black-box convention of the existing models, which only refer to flow profiles at the tray boundaries. The tray segmentation further aids in analyzing the impact of vapor flow maldistribution on the tray efficiency. The capabilities of the new model are demonstrated in two separate case studies after the model validation for perfectly mixed liquid flow in the compartments and biphasic plug flow on the tray.

Keywords: Tray efficiency modeling, flow maldistribution, stimulus-response method, axial dispersion model, residence time distribution.

1. Introduction

Non-ideal flow on cross-flow trays can significantly reduce their (Murphree) separation efficiency.[1] This is true not only for the liquid flow but also for the vapor flow. The term 'non-ideal flow' or 'flow maldistribution' refers to channeling, bypassing, recirculation, presence of stagnant zones and non-uniform velocity profiles.[2] Liquid flow patterns on the trays are complex and far from uniform flow because of the agitation caused by rising vapor, dispersion, and expanding and contracting flow path owing to circular cross-section of the column.[3] Several experimental investigations have revealed the existence of liquid maldistribution on the trays.[4-13] The stimulus-response method has been largely preferred for determining flow and mixing patterns of liquid. In this method, the liquid residence time distribution (RTD) is obtained through dispersion of tracer (e.g. dye or salt solution), which is injected in the inflowing liquid stream prior to inlet weir as an instantaneous pulse or step.[14] Different detection systems such as fiber-optic probes[9], wire-mesh sensor (WMS)[13], conductivity probes[11], and so forth have been used for transient sampling of the tracer concentration at different locations on a tray as well as at its outlet. Subsequently, the impact of these patterns on the tray efficiency can be assessed through mathematical models, revisited recently by Vishwakarma et al.[1] These models depend on parameters that are determined by tracer sampling only at the tray outlet. In other words, the conventional models are incapable of utilizing the RTD data at different locations on a tray, despite the availability of point liquid RTDs at high spatio-temporal resolution.[13] Such evaluation of the tray efficiency suggests the perception of cross-flow tray as a black box.

On the other hand, excessive hydraulic gradient in the liquid phase on a tray causes non-uniform vapor distribution, and vice-versa.[15] The vapor preferably escapes the tray through its areas with lower liquid load. It also bypasses the column through stagnant pools of liquid that evolve on consecutive trays preferably in the vicinity of the column wall.[16] However, the experimental quantification of non-uniform vapor flow in tray columns is yet to be seen in the literature. Instead, plug flow of uniform vapor composition at the tray entrance has been assumed in the conventional models.[1]

This assumption can only hold on small trays or at the lowest tray in a column i.e. next to reboiler, while it will certainly not hold on larger trays due to longer flow paths.[17,18] So far, only few authors have predicted the effects of non-uniform vapor flow on the tray efficiency through modification of the conventional models. Lewis[19] studied the effects of plug flow of liquid and vapor on the tray efficiency with the former flowing in the same as well as opposite direction on successive trays. Diener[20] extended the foregoing analysis by considering partial mixing of liquid and plug flow of vapor in respective directions on successive trays. Later, Ashley and Haselden[18] analyzed the influence of partial vapor mixing (between the trays) on the tray efficiency using mixed pool approach. Cells of perfectly mixed vapor were defined in their work analogous to pools of perfectly mixed liquid.[21] However, none of these studies considered vapor flow non-uniformity through the trays. In a subsequent study, Furzer[22] observed a reduction in the tray efficiency for linear vapor distribution and dispersed flow of liquid along the tray. For the given vapor distribution in this study, the tray efficiency corresponded to the perfectly mixed flow model and the plug flow model for perfectly mixed flow and plug flow of liquid, respectively. This means that the tray efficiency is insensitive to any vapor maldistribution for these cases of liquid flow on the tray. This observation was also reported by Lockett and Dhulesia[17] for liquid plug flow on the tray with point efficiency assumed as constant. Further, Furzer[22] and Lockett and Dhulesia[17] concluded that the vapor maldistribution results in only marginal tray efficiency loss for partially mixed liquid on the tray. In another study, Mohan et al.[15] analyzed the effect of vapor maldistribution on the tray efficiency by considering variation in the point efficiency arising from this maldistribution. Here, they observed that for perfectly mixed flow and plug flow of liquid, vapor maldistribution can significantly reduce the tray efficiency beyond that of the perfectly mixed flow model and plug flow model, respectively. Such inconsistency in efficiency predictions (even for the theoretical cases of liquid flow) demands further investigation on the influence of vapor flow patterns on the tray efficiency.

In the present work, a new model is proposed through refinement of the conventional RTD approach developed by Foss[23]. The new refined RTD (RRTD) model is capable of analyzing the impact of non-uniform flow profiles of liquid as well as vapor phase on the tray efficiency. In this work, the mathematical formulation of the RRTD model and its theoretical validation is presented in detail. In particular, the effect of biphasic flow non-idealities on the tray efficiency are studied through suitable case studies. The mathematical treatment of the tracer concentration profiles for obtaining the liquid RTD function on the tray is further described in this work.

2. Model Formulation

2.1. Background

The theory of residence time is widely accepted for studying and analyzing the flow behavior in continuous flow systems, and has found application in various fields.[24] The comprehensive and unified approach proposed by Danckwerts[25] is followed in chemical engineering. Here, the RTD of a reactor characterizes the extent of fluid mixing occurring in that reactor.[14] The fluid elements that take different routes in the reactor spend different times inside that reactor. The distribution of these times for the fluid stream exiting the reactor is represented by the RTD function, $f(t)$.[26] To determine $f(t)$, a non-reactive tracer is introduced, usually as an instantaneous pulse or step, in the feed stream at the reactor inlet. Subsequently, the time-varying concentration of the tracer in the effluent stream is monitored as shown in Fig. 1. The RTD function of a reactor during instantaneous tracer pulse injection is given by

$$f(t) = \frac{c_{out}(t)}{\int_0^\infty c_{out}(t)\, dt} \quad . \tag{1}$$

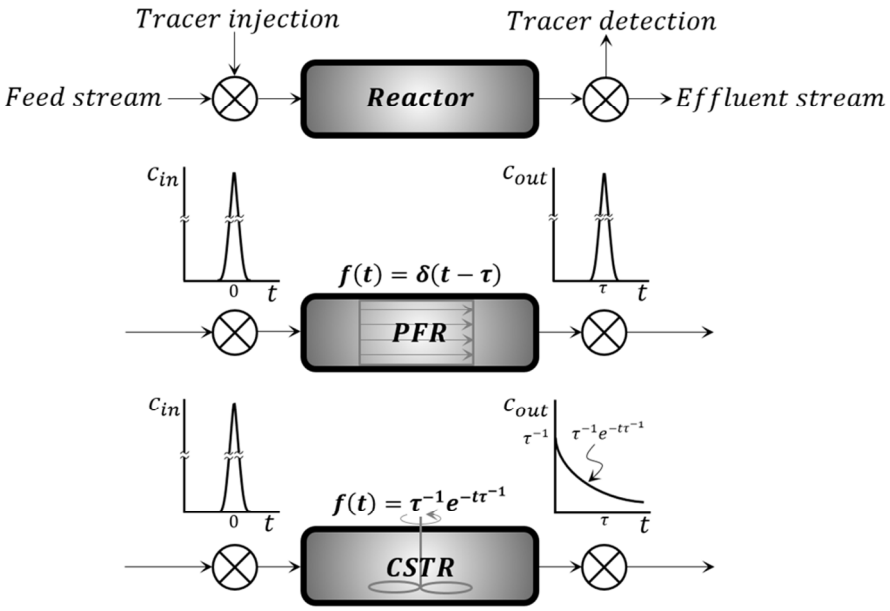

Fig. 1. Stimulus-response experiment with tracer profiles and RTD functions for ideal reactors including definitions and formulations used here.

The RTD function of the ideal reactors namely plug flow reactor (PFR) and continuous stirred-tank reactor (CSTR) are exemplarily shown in Fig. 1. During plug flow, the absence of axial mixing leads to an undistorted tracer signal at the outlet. On the contrary, the injected tracer pulse gets perfectly mixed in the CSTR, and an exponential tracer concentration distribution is obtained in the effluent stream. An instantaneous pulse of tracer with negligible dispersion between the injection point and the reactor entrance is difficult to obtain. For step tracer injection, it is difficult to maintain constant tracer concentration in the feed stream. Further, large amounts of tracer and (error inducing) differentiation of the experimental data are required to acquire RTD with the step technique.[14] Thus, to surpass these limitations, an arbitrary tracer injection near the inlet is preferred after which the RTD function can be acquired as

$$c_{out}(t) = \int_0^t c_{in}(t-t') \cdot f(t')dt' \quad . \tag{2}$$

The outlet tracer concentration is the convolution integral of the inlet tracer concentration and the reactor RTD function. An inversion of the convolution, referred to as deconvolution, is required to determine the RTD function from the injected and detected tracer concentration profiles. As deconvolution is computationally complex, different approaches have been developed for that such as Laplace and Fourier methods, flow model fitting, solution of simultaneous linear equations and so forth.[26-41] The cited literature discusses the pros and cons of these techniques in detail. The model fitting method is favored and described in this work, due to availability of the standard RTD function from the axial dispersion model (ADM).

2.2. The RTD model

Since the new model is based on refinement of the conventional RTD model, a clear understanding of the RTD model is necessary. The entire description of this model given here is directly taken from the doctoral dissertation of Foss[23]. This model employs the residence time theory by supposing that mixing of liquid produces a residence time distribution on the tray ranging from $t = 0$ to infinity. With reference to the cross-flow of liquid and vapor on the tray as displayed in Fig. 2, this model considers the following assumptions:

i. the liquid entering the tray comprises of infinite separate streams, with each stream destined to reside for a definite time on the tray,
ii. rise of uniform composition vapor with plug flow behavior through the liquid,
iii. liquid is completely mixed in the vertical direction,
iv. uniform froth height above the tray deck, and
v. linear vapor-liquid equilibrium (VLE) holds for an expected composition range.

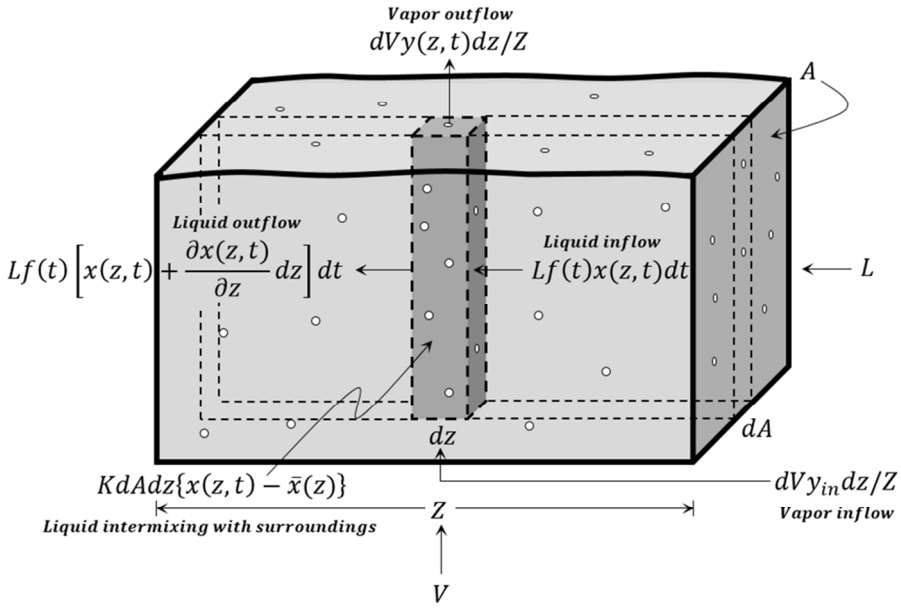

Fig. 2. Schematic representation of the RTD model.

In Fig. 2, the overall molar flow rates of liquid and vapor are represented by L and V, respectively. Here, the total froth volume on the tray is ZA, where Z is the flow path length of this tray and A is the froth cross-sectional area orthogonal to the liquid flow. The RTD function and mean residence time of liquid on the tray are given by $f(t)$ and τ, respectively. Consider a control volume (ZdA) within the froth having liquid streams that exit the tray between time t and $t + dt$. The fraction of the overall liquid flowing through the control volume is $Lf(t)dt$. As the vapor flows uniformly through the tray, the fraction of the overall vapor flowing through the control volume is dV. Using given information, the ratio of the control volume and the total froth volume can be written as

$$\frac{dA}{A} = \frac{tf(t)dt}{\tau} = \frac{dV}{V} \quad . \tag{3}$$

Eq. 3 will be used later (in Appendix A) for simplification of the material balance equation of this model. Now, consider a differential volume ($dAdz$) located at point z in the control volume as shown in Fig. 2. Here, x and y are mole fractions of the volatile component in liquid and vapor phase, respectively. The composition of volatile material in each liquid stream is affected by mass transfer to

the vapor at local point efficiency (E_{OV}) and by mass exchange with the local surrounding liquid. The mass balance on the differential element in Fig. 2 yields

$$Lf(t)dt\left\{\frac{\partial x(z,t)}{\partial z}dz\right\} + dV\{y(z,t) - y_{in}\}\frac{dz}{Z} + KdAdz\{x(z,t) - \bar{x}(z)\} = 0 \quad . \tag{4}$$

The first two terms in Eq. 4 represent the net mass transfer corresponding to liquid and vapor flow, respectively. The last term represents the intermixing of liquid in this element with the local surrounding liquid, which has been assumed as proportional to the size of differential element. Here, K denotes the coefficient of liquid intermixing per volume of the differential element. Further, $\bar{x}(z)$ is the space-mean liquid composition at point z, which is defined using Eq. 3 as

$$\bar{x}(z) = \int_0^A x(z,t)\frac{dA}{A} = \int_0^\infty x(z,t)\frac{t}{\tau}f(t)dt \quad . \tag{5}$$

Since each liquid stream is recognized by its residence time according to $f(t)$, the summation of material balance (Eq. 4) over all times can deduce the change in the liquid as well as vapor composition over the tray. This is essential for obtaining the tray efficiency. Using Eq. 3 – Eq. 5, the RTD model can be formulated as

$$E_{MV} = \frac{1 - \int_0^\infty exp(-\lambda E_{OV}\, t/\tau)\cdot f(t)dt}{\lambda \int_0^\infty exp(-\lambda E_{OV}\, t/\tau)\cdot f(t)dt} \quad . \tag{6}$$

The detailed derivation of Eq. 6 is given in Appendix A. In this equation, E_{MV} is the vapor-side Murphree tray efficiency and λ is the stripping factor. Eq. 6 can be cross-checked for plug flow and perfectly mixed flow of liquid on the tray, as the RTD function for these cases are given in Fig. 1. For plug flow, Eq. 6 transforms to the plug flow model[19], while the tray efficiency is equal to the point efficiency during perfectly mixed flow.[23] The RTD model was validated through oxygen-stripping studies on a rectangular sieve tray operated with oxygen-rich water and air.[42] This model slightly over-predicted the tray efficiency due to non-uniform froth conditions at the liquid entrance.[43] For

constant point efficiency over the tray, the rearrangement of Eq. 6 permits the application of Laplace transform, that is,

$$\int_0^\infty exp\left(-\frac{\mu t}{\tau}\right)\cdot f(t)dt = F\left(\frac{\mu}{\tau}\right) = \frac{1}{1+\mu\frac{E_{MV}}{E_{OV}}} \quad . \tag{7}$$

Here, F is the Laplace transform of $f(t)$ and $\mu(=\lambda E_{OV})$ is a dimensionless group. The prediction of the tray efficiency using Eq. 6 or Eq. 7 is straightforward, if the point efficiency and the functional form of the RTD function are known.[43] The readers are referred to the doctoral dissertation of Foss[23] for further description of this model.

2.3. The Refined RTD (RRTD) model

The refinement of the previous RTD-based efficiency prediction model, i.e. the RRTD model, starts with geometrical division of the tray into an arbitrary number of compartments in the main liquid flow direction as shown in Fig. 3. In this figure, the tray is partitioned into n compartments, which are separated from each other by the boundaries referred to as dividers. These interconnected compartments resemble the cascade of pools in the mixed pool model[21], however, dispersed liquid flow is considered in the compartments here. The liquid flows serially through the compartments, while the vapor flows through them in the direction normal to the tray deck. It is assumed that each compartment behaves like a single-pass cross-flow tray with distinct RTD and Murphree efficiency in accordance with the RTD model. In order to formulate the new model, it is compulsory to consider the following assumptions in analogy to the RTD model:

i. assumption (i) in Section 2.2 holds for every compartment,

ii. assumption (ii) in Section 2.2 holds for every compartment, however, the vapor flow rate can vary in different compartments,

iii. assumptions (iii), (iv) and (v) also hold here, and

iv. constant point efficiency over the tray

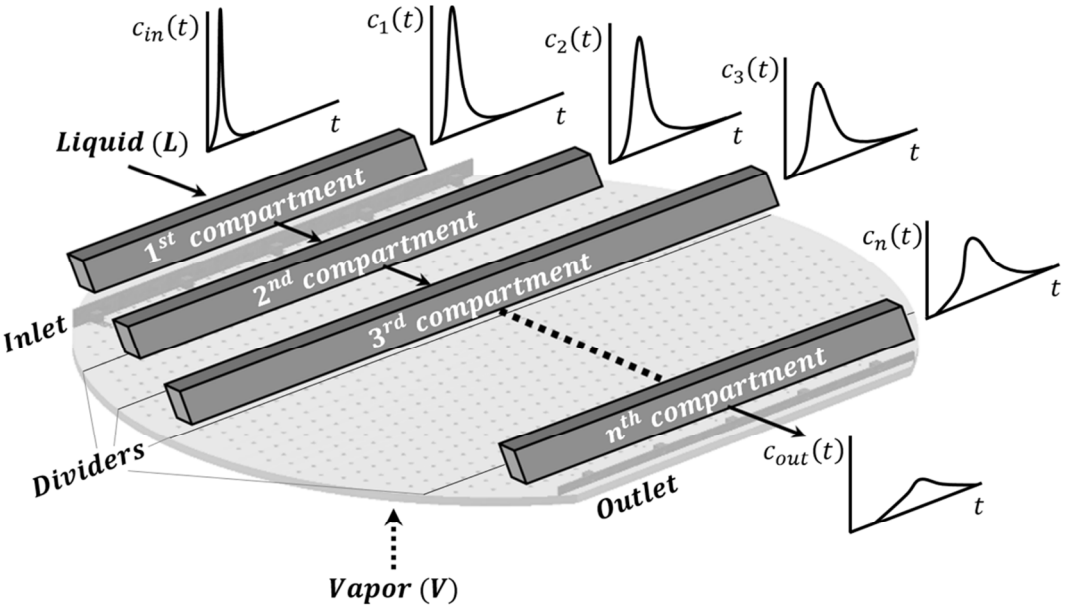

Fig. 3. Schematic representation of the RRTD model.

Each compartment (index i) has a unique RTD function $f_i(t)$ and Murphree efficiency $E_{MV,i}$. Similar to the RTD model, constant flow of liquid (L) is considered in the compartments, so that $Lf_i(t)dt$ can represent the liquid streams exiting the i^{th} compartment between time t and $t + dt$. Further, the overall vapor flow (V) is considered to be divided between n compartments as

$$V_i = a_i d_i V \quad , \tag{8}$$

such that

$$\sum_{i=1}^{n} a_i = 1 \quad , \tag{9}$$

$$\sum_{i=1}^{n} d_i = n \quad , \text{and} \tag{10}$$

$$\sum_{i=1}^{n}(a_i \cdot d_i) = 1 \quad . \tag{11}$$

$a_i\left(= A_{b,i}/A_b\right)$ and d_i are introduced as the area fraction and the vapor allocation index of the i^{th} compartment, respectively for $i = 1, 2, \ldots n$. Here, A_b and $A_{b,i}$ represent the active area of the tray and the i^{th} compartment, respectively. In simple words, the total vapor flow is distributed among the compartments depending upon their area fraction and their allocation index. This index is unity in each compartment for uniform vapor distribution over the tray. Any other distribution of this index in the compartments would represent vapor maldistribution over the tray. By following similar procedure as discussed in Section 2.2, the ratio of the control volume and the froth volume (not shown here) for the i^{th} compartment can be written as

$$\frac{dA}{A} = \frac{tf_i(t)dt}{\tau_i} = \frac{dV_i}{V_i} \quad . \tag{12}$$

The comparison of Eq. 3 and Eq. 12 leads to

$$\tau_i = a_i d_i \tau \quad . \tag{13}$$

According to Eq. 11, Eq. 13 is valid since the total residence time of liquid on the tray is the sum of its residence time in each compartment, though the actual residence time in the individual compartments could be different. Using Eq. 8, the stripping factor for the i^{th} compartment can be defined as

$$\lambda_i = b\frac{V_i}{L_i} = a_i d_i \lambda \quad , \tag{14}$$

where b is the slope of VLE line. Lockett and Dhulesia[17] reported that the point efficiency is a weak function of superficial vapor velocity. Hence, the point efficiency can be assumed as constant over the tray, regardless of any vapor maldistribution. Accordingly, the Muphree efficiency $\left(E_{MV,i}\right)$ of the i^{th} compartment through material balancing similar to Section 2.2 is

$$\frac{1}{1+\lambda_i E_{MV,i}} = \int_0^\infty exp(-\lambda_i E_{OV}\, t/\tau_i)\cdot f_i(t)dt \quad . \tag{15}$$

The application of Eq. 13, Eq. 14 and the Laplace transform in Eq. 15 results in

$$\int_0^\infty exp\left(-\frac{\mu t}{\tau}\right)\cdot f_i(t)dt = F_i\left(\frac{\mu}{\tau}\right) = \frac{1}{1+a_i d_i \mu \frac{E_{MV,i}}{E_{OV}}} \quad , \tag{16}$$

where F_i is the Laplace transform of RTD function of the i^{th} compartment. Using the RTD convolution theory as reported by Levenspiel[26] and Speight and Ozum[44], the tray RTD function is related to the compartment RTD functions as

$$f(t) = f_1(t) \otimes f_2(t) \cdots \otimes f_n(t) \quad . \tag{17}$$

The symbol $\otimes$ in the above equation represents convolution integral. Transforming Eq. 17 according to Laplace yields

$$F(s) = F_1(s)\cdot F_2(s)\cdots F_n(s) \quad . \tag{18}$$

Using $s = \mu/\tau$ in the above equation results in

$$F\left(\frac{\mu}{\tau}\right) = \prod_{i=1}^{n} F_i\left(\frac{\mu}{\tau}\right) \quad . \tag{19}$$

Substituting the Laplace functions from Eq. 7 and Eq. 16 in Eq. 19 establishes the RRTD model as

$$\frac{E_{MV}^{+}}{E_{OV}} = \frac{1}{\mu}\left[\left\{\prod_{i=1}^{n}\left(1+a_i d_i \mu \frac{E_{MV,i}}{E_{OV}}\right)\right\} - 1\right] \quad . \tag{20}$$

E_{MV}^{+} is the vapor-side tray efficiency that depends on fluid dynamics of the individual compartments through their liquid RTD functions and hence, Murphree vapor efficiencies. The superscript '+' is used here to distinguish the tray efficiency predicted by the RRTD model from that of the conventional RTD model. Similar to the conventional model, the proposed model can be assessed by verifying its predictions for perfectly mixed flow and plug flow of liquid on the tray. It is obvious that the

tray partitioning in the RRTD model makes it inapplicable for perfectly mixed liquid flow on the tray, i.e. for an equality between point and tray efficiency. However, the RRTD model transforms to the mixed pool model[21] for perfectly mixed liquid flow in the identical compartments with each compartment having vapor allocation index as unity. On the other hand, the RRTD model agrees with the plug flow model[19] for biphasic plug flow in the compartments. This is true for any vapor (allocation index) distribution over the tray. This confirms the consistency of the RRTD model prediction with the studies of Furzer[22] and Lockett and Dhulesia[17] as mentioned in Section 1. Further details regarding mathematical validation of the RRTD model are furnished in Appendix B.

3. Case Studies, Results and Analysis

3.1 Tray configuration

For application of the RRTD model, a rectangular tray (W x Z) divided into two identical and independent compartments as displayed in Fig. 4 is considered. Here, the term 'independent' means that liquid loses its memory while traversing from one compartment to the other. Therefore, a rapidly moving liquid element in the first compartment does not remember this fact in the second compartment, and hence does not flow preferentially faster or slower there.[26] The tray boundaries in the liquid flow direction are referred to as inlet and outlet, while the tray bisector is referred to as divider. Liquid and vapor load on this tray are L and V, respectively. The area fraction and the vapor allocation index for the identical compartments with uniform vapor flow are $a_1 = a_2 = 0.5$ and $d_1 = d_2 = 1$, respectively. The numerical values of these parameters satisfy Eq. 9 to Eq. 11.

In RRTD model, the process of tray efficiency prediction starts with obtaining the liquid RTD function in the compartments. The time-dependent concentration profiles of tracer are defined at compartment boundaries, similar to the stimulus-response method discussed in Section 2.1, to obtain the RTD function using Eq. 2. In this work, the profile of the inlet tracer concentration is inspired

from the WMS experiment conducted by Schubert et al.[13] for flow characterization in an air-water sieve tray column simulator of 800 mm diameter using salt solution as tracer. The standard RTD function (i.e. Gaussian error function) through solution of the ADM for open-open boundary condition is available in the literature[26,45] as

$$f(t) = \sqrt{\frac{1}{4\pi t \tau_h N_{TD}}} \cdot exp\left\{ -\frac{\left(1 - \frac{t}{\tau_h}\right)^2}{\frac{4tN_{TD}}{\tau_h}} \right\} \quad . \tag{21}$$

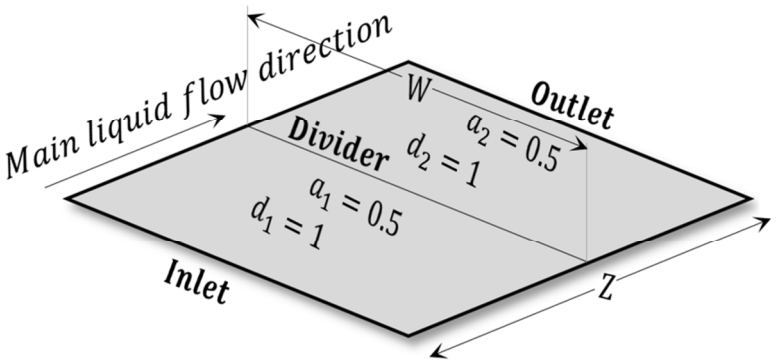

Fig. 4. Tray framework for the RRTD model.

Here, τ_h is the hydraulic or space-time that is based on bulk liquid velocity and flow path length (Z). N_{TD} is the dimensionless parameter named, according to the suggestion of Levenspiel[26], as tray dispersion number whose definition[14,26] is

$$N_{TD} = \frac{D_E \cdot \tau_h}{Z_1^2} \quad . \tag{22}$$

Mostly, the reciprocal of tray dispersion number is referred to as Péclet number in the literature. The usage of the term 'Péclet number' has been criticized by Levenspiel[26]. Here, D_E is the eddy diffusion coefficient that characterizes liquid backmixing in a system. A desired RTD function can be assigned to a compartment by assuming N_{TD} and τ_h in Eq. 21. As inlet concentration profile is derived

from the WMS study[13], defining the outlet or divider concentration profile is possible using Eq. 2. On the contrary, deconvolution is required to acquire the RTD function for a given set of inlet-outlet, inlet-divider and divider-outlet concentration profiles. The flowchart in Appendix C (Fig. A2) summarizes the algorithm that employs non-linear least square fitting method and Eq. 21 to achieve deconvolution in this work. The correctness of this algorithm can be ensured using the definitions given in Tab. 1 as validating criteria. This table summarizes the mean residence time τ and the variance σ^2 that can be calculated from the RTD function. These quantities must agree with their definitions given for the ADM in Tab. 1. In addition, Tab. 1 can be used to calculate N_{TD} and τ_h for a given RTD function on the tray. Further, the computed RTD function should also agree with the tank in series (TIS) model for an integral number of tanks ($\tilde{n}$) in the main liquid flow direction. However, this criterion is only valid when the liquid flow on a tray or compartment does not deviate considerably from plug flow.[26] It must be noted that $\tilde{n}$ corresponds to integral number of ideal CSTRs in the liquid flow direction in TIS model, which can be different from the number of compartments (n) in the RRTD model.

Tab. 1. Definitions for validating the deconvolution calculation.

Term	Usual definition	ADM, open-open system
$\boldsymbol{\tau}$	$\int_0^\infty t \cdot f(t)dt$	$\tau_h \cdot (1 + 2N_{TD})$
$\boldsymbol{\sigma^2}$	$\int_0^\infty (t-\tau)^2 \cdot f(t)dt$	$\tau_h^2 \cdot (2N_{TD} + 8N_{TD}^2)$
$\boldsymbol{f(t)}$	Tanks in series model $\frac{t^{\tilde{n}-1} \cdot \tilde{n}^{\tilde{n}} \cdot exp(-\tilde{n}t/\tau)}{\tau^{\tilde{n}} \cdot (\tilde{n}-1)!}$	
	where $\tilde{n} = \left\lceil 1 + \frac{1}{2N_{TD}} \right\rceil$	

Earlier, the point efficiency has been considered as constant over the tray in the RRTD model. Instead of defining liquid flow rate (L), vapor flow rate (V) and slope of the VLE line (b) separately, the dimensionless group λE_{OV} has been defined in this work. Further, the liquid RTD function in the tray compartments are assumed to be valid for the considered λE_{OV}. Besides, λE_{OV} influences the cross-flow liquid mixing on a tray.[8] According to Vishwakarma et al.[1], higher liquid mixing orthogonal to the liquid flow direction and higher resistance to the detrimental vapor bypassing can be expected for an increase in λE_{OV}.

3.2 Effect of different compartment RTD functions on the tray efficiency during uniform vapor distribution

3.2.1 Tracer concentration and RTD profiles

Firstly, dispersion number and hydraulic time are needed for the bisected tray with uniform vapor distribution (shown in Fig. 4) for defining the tray RTD function using Eq. 21. The numerical value of these parameters are arbitrarily selected as 0.05 and 20 s, respectively. Convolution integral of the inlet tracer concentration (derived from the WMS monitored tracer experiment[13]) and the RTD function provides the outlet tracer concentration. Inlet and resulting outlet tracer concentration profile and the tray RTD function are shown in Fig. 5a and Fig. 5b, respectively. All these data are sufficient to utilize the conventional RTD model[23] and predict the tray efficiency for the assumed λE_{OV}.

For application of the RRTD model, the aforementioned procedure is followed for assigning the tracer concentration profile at the divider by assuming N_{TD} and τ_h in the first compartment. Then, deconvolution is performed, as discussed in Section 3.1, for computing the RTD function and its parameters in the second compartment. This allows predicting Murphree efficiency of the bisected tray using the RRTD model for assumed λE_{OV}. Three arbitrary concentration profiles (cases I to III)

at the divider, by assuming different N_{TD} and τ_h in the first compartment, are considered and shown in Fig. 5a. Inlet and outlet concentration profiles of the tray are the same regardless of the divider profiles. In other words, the overall RTD function of the tray remains the same in all three cases. This permits comparing the tray efficiency predictions from the RTD model and the RRTD model. A noticeable difference in the compartment RTD functions for the three cases and the tray RTD function is apparent in Fig. 5b. Hence, significant difference in the tray efficiency is anticipated for these cases, which is crucial for justifying the sensitivity of the RRTD model to intermediary flow conditions unlike in the conventional RTD model.

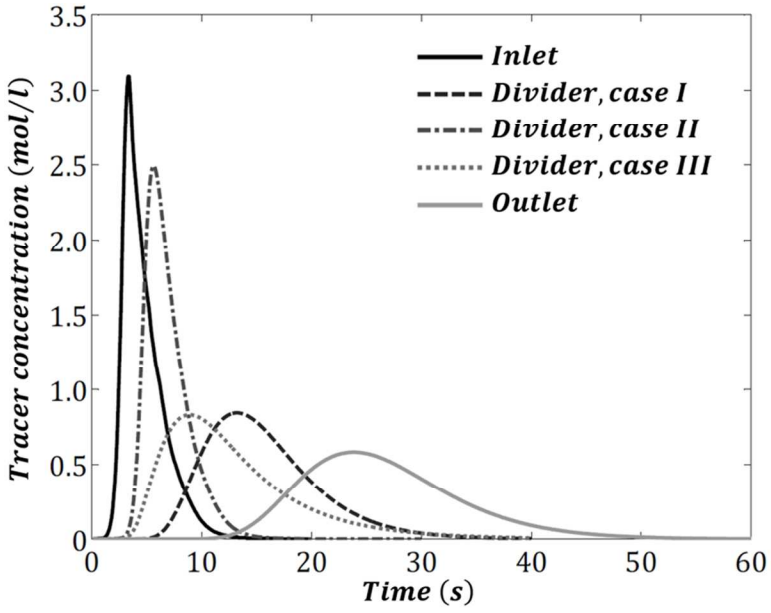

(a)

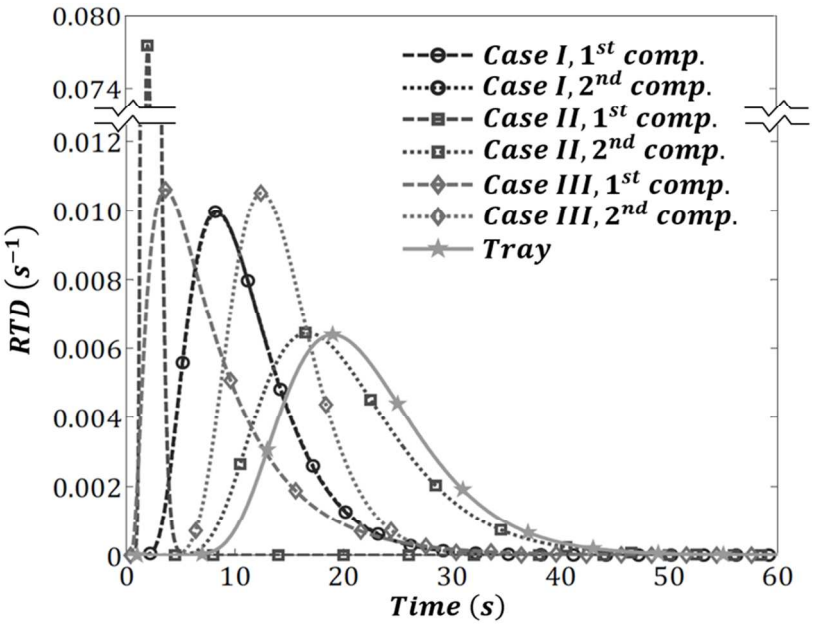

(b)

Fig. 5. (a) Time-varying profiles of tracer concentration at the compartment boundaries, and (b) RTD functions in the compartments with identical vapor load.

Tab. 2. Numerical description of RTD parameters in the tray compartments.

System		N_{TD} **x 100** $(-)$	τ_i (s)	$\left\|\frac{\tau - (\sum \tau_i)}{\tau}\right\|$ **x 100** (%)
Tray		5	$(\tau =)$ 22	–
Case I	Compartment 1	10	11	0.23
	Compartment 2	10.02	11.05	
Case II	Compartment 1	3.03	2.23	1.09
	Compartment 2	6.25	20.01	
Case III	Compartment 1	33.33	8.33	2.18
	Compartment 2	4.33	14.15	

Case I corresponds to uniform liquid mixing in both compartments, where the dispersion number and the mean residence time are kept almost identical. Hence, the RTD curve of both compartments in this case coincide in Fig. 5b. Note that small deviations in the numerical values of RTD parameters here result from deconvolution operation in the second compartment. Case II considers less liquid mixing in the first compartment, which is evident from the steep RTD profile in Fig. 5b. Consequently, a comparatively short and wide RTD curve is encountered in the second compartment in this case, as the compartment RTD functions have to comply with Eq. 17 in each case. The same is applicable for the compartment RTD profiles in case III, where intense liquid mixing is prescribed in the first compartment. Tab. 2 summarizes the RTD parameters in the compartments for each case as well as for the tray. The maximum difference between the sum of mean liquid residence time in the compartments and the overall tray residence time for these cases is approximately 2%, which is induced by deconvolution calculations. Hence, the additive property of the liquid residence time in the compartments arranged serially along the flow direction, as suggested by Levenspiel[26], holds in this study. Further, Levenspiel and Smith[45] reported the increase in skewness of the RTD function with increasing dispersion number. This can be observed in Tab. 2 and Fig. 5b for the first compartment in case III, where the dispersion number and the skewness of the RTD curve are highest.

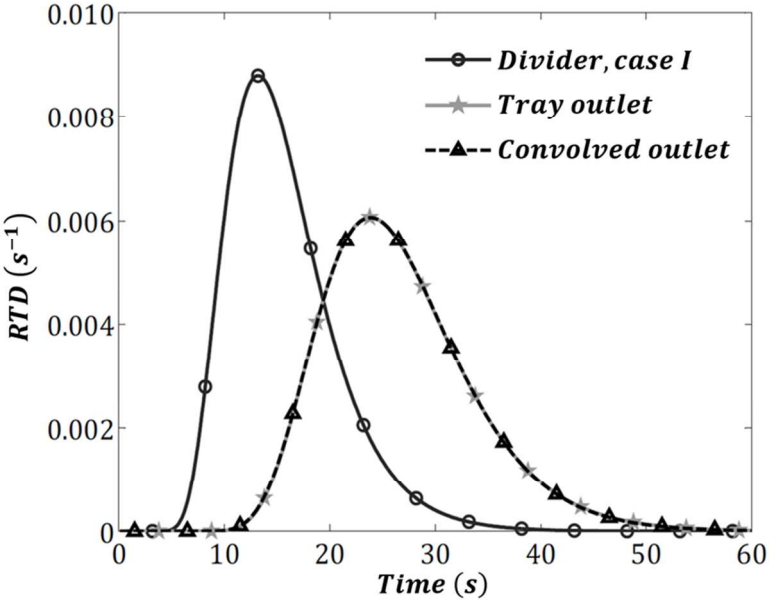

(a)

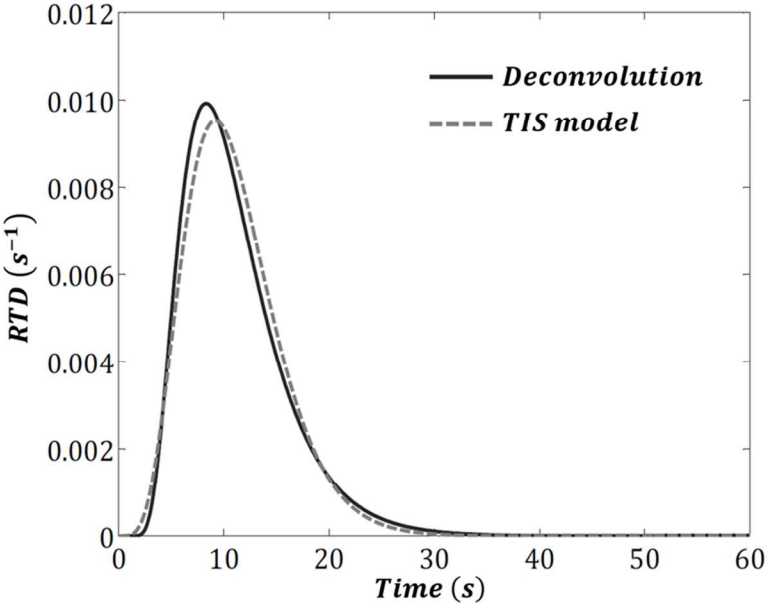

(b)

Fig. 6. (a) RTD profiles at the boundaries and (b) comparison of the compartment RTD function with tanks in series (TIS) model for second compartment of case I.

As previously discussed, the correctness of the computation can be proven through the validating criteria given in Tab. 1. The second compartment of case I (Tab. 2) is arbitrarily selected for showing the validity of its RTD profile and associated parameters. For this compartment, the mean residence time and the variance of the RTD function and that from the ADM perfectly match each other with their numerical values as 11.05 s and 23.79 s^2, respectively. Moreover, the graphical validation of the RTD profile of this compartment is shown in Fig. 6a and Fig. 6b. Convolved RTD profile (using the compartment and divider RTD profiles) and actual outlet RTD profile agree very well (Fig. 6a). The compartment RTD profile obtained from deconvolution also agrees with the TIS model (Fig. 6b), except little deviation in the distribution peaks. This is because the liquid flow in this compartment deviates considerably from the plug flow, which is evident from its dispersion number given in Tab. 2. Besides, the same criteria hold true for all other cases (not shown here), which justifies the validity of the RTD profiles and the related parameters in this work.

3.2.2 Tray efficiency predictions using the RRTD model and the RTD model

The employment of liquid RTD function and mean residence time of the whole tray, as given in Fig. 5b and Tab. 2, respectively, in the RTD model yields the tray efficiency for the assumed λE_{OV}. The same approach is used to obtain the efficiency of the compartments of the bisected tray. Subsequently, the RRTD model (Eq. 20) is employed to forecast the tray efficiency by conjoining the compartmental efficiencies in each of the three cases for the assumed λE_{OV}. Fig. 7 presents the tray efficiency predictions using the RTD model and the RRTD model, where the upper limit of the efficiency ratio is given by the plug flow model[19]. At first, the difference in the efficiency predictions for the given cases can be seen in this figure, though the overall liquid RTD function on the tray is the same in all cases. The tray efficiency predictions from the RTD model and for case I using the RRTD model are consistent with each other, because every compartment in this case imitates half of the tray as known from their dispersion number and residence time (see Tab. 2). As the magnitude of liquid

dispersion and residence time are almost same in both compartments, their Murphree efficiencies are consequently same in this case. Thus, it can be concluded that the RTD model inherently considers a tray to be comprised of finite number of identical compartments in the main liquid flow direction with uniform liquid mixing and residence time for its efficiency predictions. The consideration of uniform liquid mixing in the equisized compartments along the liquid flow direction indicates the analogy between the RTD model and the mixed pool model[21]. However, this is appropriate only for uniform distribution of vapor flow over the tray.

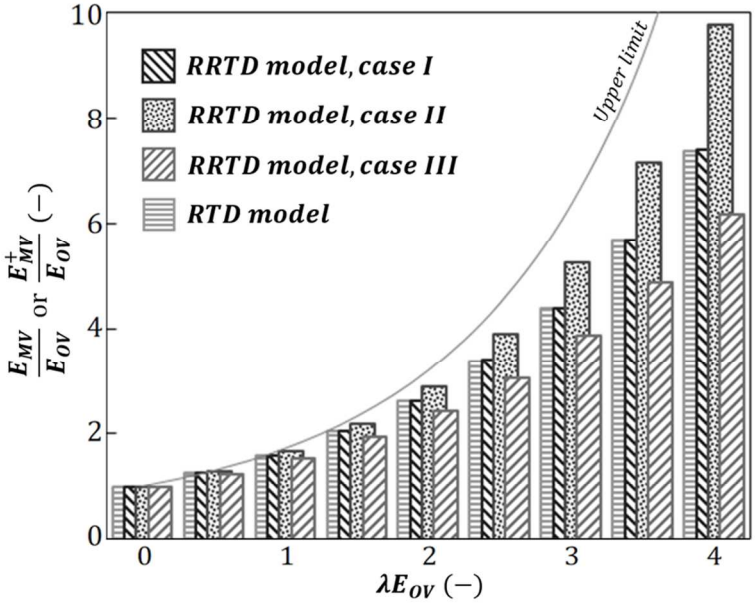

Fig. 7. Tray efficiency predictions using RTD model and RRTD model.

Lockett and Safekourdi[2] suggested that liquid backmixing on the tray is detrimental for its efficiency.[1] Accordingly, the higher is the dispersion number of tray or compartment, the lower is its Murphree efficiency. For case II, the efficiency of the first compartment is very high due to low dispersion in the flow direction. As the RTD function of this compartment approximately resembles the impulse response of a PFR (as shown in Fig. 1), its efficiency approaches the solution of the plug

flow model[19]. Combining the efficiency of this compartment with that of the second compartment (having moderate liquid dispersion) using the RRTD model leads to the tray efficiency predictions for case II. In this case, the efficiency predictions from the RRTD model are higher than that of the RTD model. In case III, the dispersion number in the first compartment is very high. The RTD function of this compartment is approaching the impulse response of an ideal CSTR (as shown in Fig. 1), so the compartmental efficiency remains close to the point efficiency. Though the backmixing in the second compartment is comparatively low, the resulting tray efficiency predictions from the RRTD model for case III are lower than that of the RTD model. Besides, the tray efficiency predictions from the RTD model and the RRTD model for all three cases are similar for $\lambda E_{OV} \leq 1$. According to Vishwakarma et al.[1], at higher λE_{OV}, intensified liquid mixing orthogonal to its flow direction and higher resistance to vapor bypassing is expected, which is beneficial for the tray efficiency. The rise in the tray efficiency prediction with increasing λE_{OV} will be significantly higher for the case with less liquid backmixing. Thus, the difference in the efficiency predictions from the RRTD model and the RTD model becomes apparent for $\lambda E_{OV} > 1$. At $\lambda E_{OV} = 4$, the tray efficiency prediction by the RRTD model for case II and case III is approximately 33% higher and 16% lower than that from the RTD model, respectively. These observations confirm the RRTD model's susceptibility to axial mixing behavior of liquid at intermediate locations on the tray.

3.3 Effect of non-uniform vapor distribution on the tray efficiency

3.3.1 Tray configuration with tracer concentration and RTD profiles

For assessing the impact of non-uniform vapor flow on the tray efficiency, a rectangular tray similar to Fig. 4 is considered as shown in Fig. 8a. Here, the tray is divided into three identical and independent compartments, each with the area fraction of $a_1 = a_2 = a_3 = 0.3\overline{3}$. Dividing a tray into three or more compartments is essential for signifying the effect of different degrees of vapor mal-

distribution on the tray efficiency. The dividers between inlet and outlet of the tray in the main liquid flow direction are called as divider 1 and divider 2.

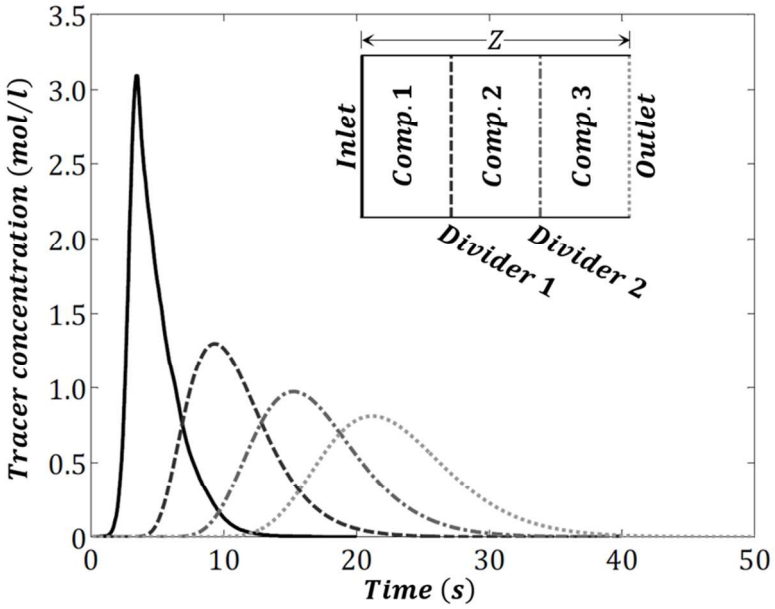

(a)

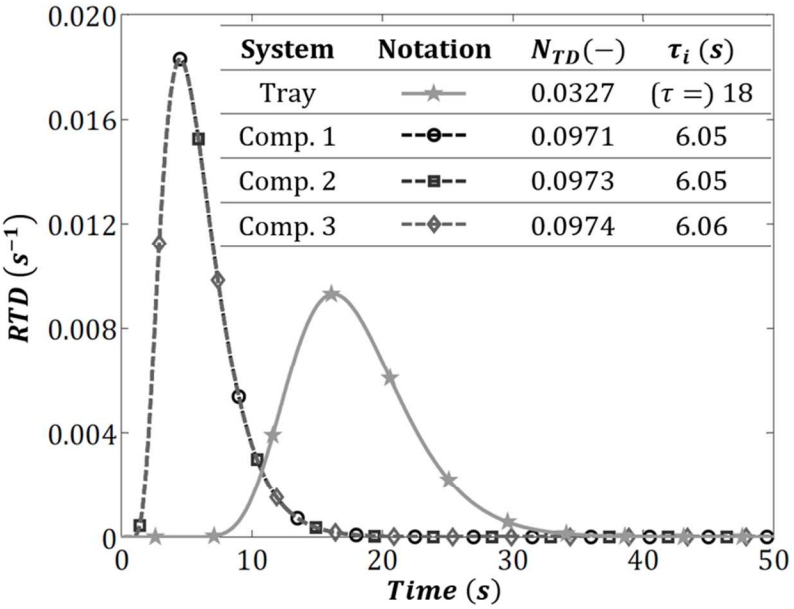

(b)

Fig. 8. (a) Tracer concentration profiles at the compartment boundaries and (b) RTD function with related parameters for each compartment of the trisected tray.

The tracer concentration profile at the inlet as shown in Fig. 5a is retained for the trisected tray. Dispersion number and mean residence time of liquid on the tray are selected as 3.27 x 10^{-2} and 18 s, respectively. This allows obtaining the tray RTD function and eventually the tracer concentration profile at the outlet using Eq. 2. The tracer concentration profile at divider 1 and 2 are defined by considering uniform liquid dispersion in the compartments, while maintaining the profiles at inlet and outlet of the tray. The concentration profiles at the compartment boundaries and the liquid RTD function in the compartments are presented in Fig. 8a and Fig. 8b, respectively. Dispersion number and mean residence time considered in every compartment are also summarized in Fig. 8b. Similar to the previous section, these RTD functions are assumed to be valid for the presumed dimensionless group λE_{OV}, since the point efficiency and the stripping factor are also considered as constant over the tray.

Uniform spreading and diminishing (peak height) of tracer profiles in the liquid flow direction on the tray is apparent in Fig. 8a. This is obvious because of similar dispersion number and liquid residence time in the compartments. Accordingly, their RTD functions overlap each other as shown in Fig. 8b. Further, the difference between the sum of liquid residence time in the compartments and the overall residence time is less than 1%, which justifies the earlier mentioned additive property of the residence time.[26] The validating criteria given in Tab. 1 also hold perfectly for the given RTD profiles and their parameters, except slight deviation in the peak of the RTD curves compared to that of the TIS model (not shown here but similar to Fig. 6b).

The distribution of vapor allocation index in the compartments represents the vapor flow profile through the tray. As mentioned in Section 2.3, this index is unity in all compartments for uniformly distributed vapor over the tray, and any other distribution of this index represents non-uniform vapor flow. Four different cases of vapor flow namely uniform distribution (1, 1, 1), mild channeling (0.75, 1.5, 0.75), moderate channeling (0.5, 2, 0.5) and severe channeling (0.25, 2.5, 0.25) are considered in this study. The numerical values inside parentheses define the allocation index in the compartments in serial order for each case, which are also illustrated in Fig. 9. The numerical values of the area fraction and the allocation index here satisfy Eq. 9 to Eq. 11. The degree of maldistribution in the overall vapor flow (or in other words, the deviation from uniform vapor distribution) is low for mild channeling, intermediate for moderate channeling and high for severe channeling.

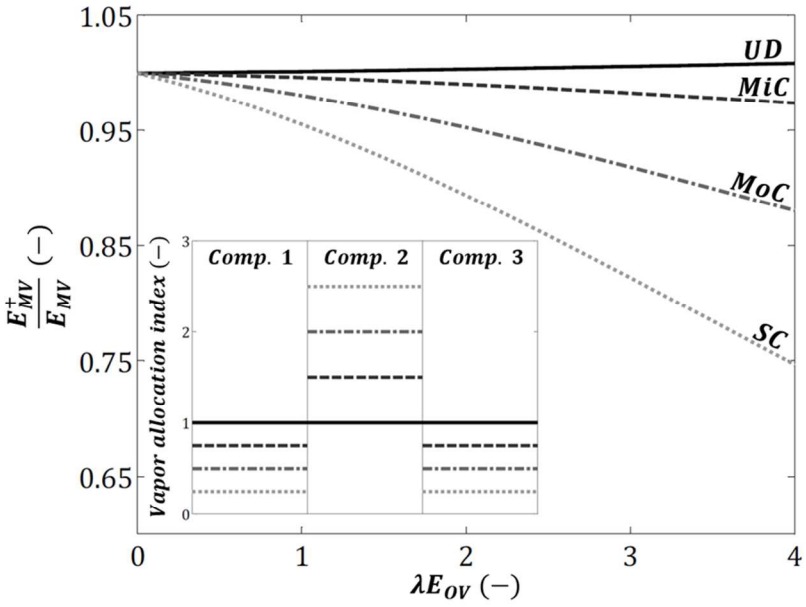

Fig. 9. Tray efficiency predictions during non-uniform vapor distribution (the terms UD, MiC, MoC and SC stand for uniform distribution, mild channeling, moderate channeling and severe channeling, respectively).

3.3.2 Comparison of tray efficiency predictions from the RRTD model and the RTD model

As the RTD model is irresponsive to any vapor flow maldistribution, its efficiency predictions are considered as reference for depicting the impact of non-uniform vapor flow on the tray efficiency using the RRTD model. The ratio of tray efficiency predictions from the RRTD model and the RTD model are displayed in Fig. 9 for assumed λE_{OV}. The RRTD model predictions are consistent with that of the RTD model during uniform flow of vapor in the compartments. For this distribution, the maximum difference between the models' predictions is 0.84% at $\lambda E_{OV} = 4$, which is exclusively caused by the deconvolution calculations. The agreement in the predictions from the two models for uniform dispersion number and residence time in the compartments with same amount of vapor flow is also reported in Section 3.2.2. Further, Fig. 9 shows the adverse effects of vapor channeling on the tray separation performance. The decline in the separation efficiency is an outcome of vapor

channeling through the tray. In other words, larger is the deviation from uniform vapor distribution, higher is the tray efficiency loss. As already mentioned, increasing λE_{OV} results in higher resistance to vapor bypassing, which increases the tray efficiency.[1] However, this improvement in the efficiency is high during uniform distribution, while it is not so high during mild channeling, low during moderate channeling and the lowest during severe channeling. Accordingly, the ratio of RRTD and RTD model predictions decline with increasing λE_{OV} for the given cases in Fig. 9. The difference between the predictions from the two models during vapor channeling is highest at $\lambda E_{OV} = 4$. At this λE_{OV}, the tray efficiency according to the RRTD model during mild, moderate and severe channeling is approximately 3%, 13% and 26% lower than that of the RTD model, respectively. Therefore, unlike the RTD model, the RRTD model is capable of accounting for the adverse effects of vapor maldistribution on the tray efficiency. Furzer[22] and Lockett and Dhulesia[17] reported only minor losses of the tray efficiency during vapor maldistribution. The present investigation supports their conclusion only for mild vapor channeling through the tray.

4. Conclusion

A new model, called RRTD model, based upon the refinement of the conventional RTD approach has been proposed in this work. Mathematical formulation of the RRTD model involves geometrical partitioning of a tray into compartments along the main liquid flow direction. This partitioning permits accounting for the impact of liquid mixing behavior at intermediate tray locations on the tray efficiency. This breaks the black-box convention of the former efficiency assessment by conventional models, which refer to flow profiles at the tray boundaries only. The RRTD model has been validated mathematically for perfectly mixed flow in the compartments and plug flow on the tray. Unlike existing approaches that consider only uniform vapor distribution over the tray, the proposed model can predict the impact of non-uniform vapor flow on the tray efficiency.

The existing air-water sieve tray column (800 mm diameter) mockup facility is currently being modified in order to obtain the RTD profiles at various locations on the tray. In addition, this facility will be used for evaluating mass-transfer performance of the tray during flow conditions identical to that of RTD experiment. Eventually, this will enable experimental validation of the RRTD model in the future.

Acknowledgment

This work was supported by the German Academic Exchange Service (Deutscher Akademischer Austauschdienst, DAAD) [grant number 91563198].

Nomenclature

A	Cross-sectional area of froth perpendicular to the main liquid flow direction (m^2)
A_b	Bubbling or perforated area (m^2)
a	Area fraction of the tray compartment (-)
b	Slope of the VLE line (-)
$c(t)$	Time-dependent tracer concentration (mol/m^3)
D_E	Eddy diffusion coefficient (m^2/s)
d	Vapor allocation index in the tray compartment (-)
E_{ML}	Liquid-side Murphree tray efficiency (-)
E_{MV}	Vapor-side Murphree tray efficiency (-)
E_{OV}	Vapor-side point efficiency (-)
F	Laplace function (-)
$f(t)$	Residence time distribution function (s^{-1})
h_f	Froth height (m)

i	Index for the tray compartments (-)
K	Intermixing coefficient per volume of differential element in the RTD model (mol/(m^3·s))
L	Liquid flow rate (mol/s)
N_{TD}	Tray dispersion number (-)
n	Number of compartments in the main liquid flow direction (-)
$\tilde{n}$	Number of ideal CSTRs in the main flow direction in tanks in series model (-)
p	Parameter used in the Appendix A $(= z/Z)$ (-)
$R(t)$	Response function $\left(= c(t)/\int_0^\infty c(t)\,dt\right)$ (s^{-1})
s	Frequency variable (s^{-1})
t	Time (s)
V	Vapor or gas flow rate (mol/s)
W	Weir length (m)
x	Composition (mole fraction) of the volatile component in the liquid phase (-)
$\bar{x}(z)$	Space mean composition of liquid at point z (-)
y	Composition (mole fraction) of the volatile component in the vapor phase (-)
Z	Flow path length (m)
z	Distance from inlet weir in the main liquid flow direction (m)

Subscripts

b	Bubbling or perforated area of the tray
i	Index for the tray compartments
in	Inlet
m	mth tray
out	Outlet

Superscript

$+$	Indicator for tray efficiency derived from the RRTD model

Greek Letters

λ	Stripping factor ($= bV/L$) (-)
μ	Non-dimensional parameter ($= \lambda E_{OV}$) (-)
τ	Mean residence time of liquid on the tray (s)
τ_h	Hydraulic or space time (s)

Abbreviations

ADM	Axial dispersion model
$CSTR$	Continuous stirred-tank reactor
PFR	Plug flow reactor
RTD	Residence time distribution
TIS	Tanks in series
VLE	Vapor-liquid equilibrium
WMS	Wire-mesh sensor

References

1. Vishwakarma V, Schubert M, Hampel U. Assessment of separation efficiency modeling and visualization approaches pertaining to flow and mixing patterns on distillation trays. *Chemical Engineering Science.* 2018;185:182-208.
2. Lockett MJ, Safekourdi A. The effect of the liquid flow pattern on distillation plate efficiency. *Chemical Engineering Journal.* 1976;11(2):111-121.
3. Górak A, Sorensen E. *Distillation: fundamentals and principles.* Academic Press; 2014.
4. Stichlmair J, Ulbrich S. Liquid channelling on trays and its effect on plate efficiency. *Chemical Engineering and Technology.* 1987;10(1):33-37.
5. Biddulph MW, Bultitude DP. Flow characteristics of a small-hole sieve tray. *AIChE Journal.* 1990;36(12):1913-1916.
6. Sohlo J, Kinnunen S. Dispersion and flow phenomena on a sieve plate. *Transactions of the Institution of Chemical Engineers.* 1977;55:71-73.
7. Porter KE, Yu KT, Chambers S, Zhang MQ. Flow patterns and temperature profiles on a 2.44 m diameter sieve tray. *Chemical Engineering Research and Design.* 1992;70(A):489-500.
8. Porter KE, Lockett MJ, Lim CT. The effect of liquid channeling on distillation plate efficiency. *Transactions of the Institution of Chemical Engineers.* 1972;50(2):91-101.
9. Solari RB, Bell RL. Fluid flow patterns and velocity distribution on commercial-scale sieve trays. *AIChE Journal.* 1986;32(4):640-649.
10. Li Y, Wang L, Yao K. New technique for measuring fluid flow patterns on a multiple downcomer tray. *Industrial and Engineering Chemistry Research.* 2007;46(9):2892-2897.
11. Yu KT, Huang J, Li JL, Song HH. Two-dimensional flow and eddy diffusion on a sieve tray. *Chemical Engineering Science.* 1990;45(9):2901-2906.
12. Liu C, Yuan X, Yu KT, Zhu X. A fluid–dynamic model for flow pattern on a distillation tray. *Chemical Engineering Science.* 2000;55(12):2287-2294.

13. Schubert M, Piechotta M, Beyer M, Schleicher E, Hampel U, Paschold J. An imaging technique for characterization of fluid flow pattern on industrial-scale column sieve trays. *Chemical Engineering Research and Design.* 2016;111:138-146.

14. Fogler HS, Gürmen MN. *Elements of chemical reaction engineering (online version).* 4th ed: University of Michigan; 2008.

15. Mohan T, Rao KK, Rao DP. Effect of vapor maldistribution on tray efficiency. *Industrial and Engineering Chemistry Process Design and Development.* 1983;22(3):376-380.

16. Brambilla A. The effect of vapour mixing on efficiency of large diameter distillation plates. *Chemical Engineering Science.* 1976;31(7):517-523.

17. Lockett MM, Dhulesia HA. Murphree plate efficiency with nonuniform vapour distribution. *Chemical Engineering Journal.* 1980;19(3):183-188.

18. Ashley MJ, Haselden GG. The calculation of plate efficiency under conditions of finite mixing in both phases in multiplate columns, and the potential advantage of parallel flow. *Chemical Engineering Science.* 1970;25(11):1665-1672.

19. Lewis Jr WK. Rectification of binary mixtures. *Industrial and Engineering Chemistry.* 1936;28(4):399-402.

20. Diener D. Calculation of effect of vapor mixing on tray efficiency. *Industrial and Engineering Chemistry Process Design and Development.* 1967;6(4):499-503.

21. Gautreaux MF, O'Connell HE. Effect of length of liquid path on plate efficiency. *Chemical Engineering Progress.* 1955;51(5):232-237.

22. Furzer I. The effect of vapor distribution on distillation plate efficiencies. *AIChE Journal.* 1969;15(2):235-239.

23. Foss AS. *Liquid mixing on bubble trays and its effect upon plate efficiency* [Doctoral dissertation], University of Delaware; 1957.

24. Nauman EB. Residence time theory. *Industrial and Engineering Chemistry Research.* 2008;47(10):3752-3766.

25. Danckwerts PV. Continuous flow systems: distribution of residence times. *Chemical Engineering Science.* 1953;2(1):1-13.

26. Levenspiel O. *Chemical reaction engineering.* 3rd ed: John Wiley and Sons; 1999.

27. Azizi F, Abou Hweij K. Liquid-phase axial dispersion of turbulent gas–liquid co-current flow through screen-type static mixers. *AIChE Journal.* 2017;63(4):1390-1403.

28. Thakur R, Vial C, Nigam K, Nauman E, Djelveh G. Static mixers in the process industries—a review. *Chemical Engineering Research and Design.* 2003;81(7):787-826.

29. Häfeli R, Hutter C, Damsohn M, Prasser H-M, von Rohr PR. Dispersion in fully developed flow through regular porous structures: experiments with wire-mesh sensors. *Chemical Engineering and Processing: Process Intensification.* 2013;69:104-111.

30. Bennia A, Nahman N. Deconvolution of system impulse responses and time domain waveforms. *IEEE Transactions on Instrumentation and Measurement.* 1990;79:933-939.

31. Bošković D, Loebbecke S. Modelling of the residence time distribution in micromixers. *Chemical Engineering Journal.* 2008;135:S138-S146.

32. Essadki AH, Gourich B, Vial C, Delmas H. Residence time distribution measurements in an external-loop airlift reactor: Study of the hydrodynamics of the liquid circulation induced by the hydrogen bubbles. *Chemical Engineering Science.* 2011;66(14):3125-3132.

33. Heibel AK, Lebens PJ, Middelhoff JW, Kapteijn F, Moulijn J. Liquid residence time distribution in the film flow monolith reactor. *AIChE journal.* 2005;51(1):122-133.

34. Hutter C, Zenklusen A, Lang R, von Rohr PR. Axial dispersion in metal foams and streamwise-periodic porous media. *Chemical Engineering Science.* 2011;66(6):1132-1141.

35. Mills P, Duduković M. Convolution and deconvolution of nonideal tracer response data with application to three-phase packed-beds. *Computers and Chemical Engineering.* 1989;13(8):881-898.

36. Mao Z-S, Xiong T, Chen J. Residence time distribution of liquid flow in a trickle bed evaluated using FFT deconvolution. *Chemical Engineering Communications.* 1998;169(1):223-244.

37. Parruck B, Riad SM. Study and performance evaluation of two iterative frequency-domain deconvolution techniques. *IEEE Transactions on Instrumentation and Measurement.* 1984;33(4):281-287.

38. Pananakis D, Abel E. A comparison of methods for the deconvolution of isothermal DSC data. *Thermochimica Acta.* 1998;315(2):107-119.

39. Saber M, Pham-Huu C, Edouard D. Axial dispersion based on the residence time distribution curves in a millireactor filled with β-SiC foam catalyst. *Industrial and Engineering Chemistry Research.* 2012;51(46):15011-15017.

40. Gutierrez CG, Dias EF, Gut JA. Residence time distribution in holding tubes using generalized convection model and numerical convolution for non-ideal tracer detection. *Journal of Food Engineering.* 2010;98(2):248-256.

41. Georget E, Sauvageat JL, Burbidge A, Mathys A. Residence time distributions in a modular micro reaction system. *Journal of Food Engineering.* 2013;116(4):910-919.

42. Foss A, Gerster J. Liquid film efficiencies on sieve trays. *Chemical Engineering Progress.* 1956;52(1):28.

43. Foss AS, Gerster JA, Pigford RL. Effect of liquid mixing on the performance of bubble trays. *AIChE Journal.* 1958;4(2):231-239.

44. Speight JG, Ozum B. *Petroleum refining processes.* CRC Press; 2001.

45. Levenspiel O, Smith W. Notes on the diffusion-type model for the longitudinal mixing of fluids in flow. *Chemical Engineering Science.* 1957;6(4-5):227-235.

Appendix A: Mathematical treatment in the RTD model

The material balance over the differential element in Fig. 2 results in

$$Lf(t)dt\left\{\frac{\partial x(z,t)}{\partial z}dz\right\}+dV\{y(z,t)-y_{in}\}\frac{dz}{Z}+KdAdz\{x(z,t)-\bar{x}(z)\}=0 \quad . \tag{4}$$

Eq. 3 permits to eliminate dA and dV in the above equation. Using the usual definition of the point efficiency, stripping factor and linear VLE relationship, and assuming $p=z/Z$ in Eq. 4 leads to

$$f(t)\left[\frac{dx(p,t)}{dp}+\lambda E_{OV}\frac{t}{\tau}\{x(p,t)-x_e^*\}+\frac{KAZ}{L}\frac{t}{\tau}\{x(p,t)-\bar{x}(p)\}\right]dt=0 \quad . \tag{A1.1}$$

Substituting the space-mean liquid composition in the above equation by that given in Eq. 5 and integrating the resulting equation with respect to t over full range of time gives

$$\int_0^\infty f(t)\left[\frac{dx(p,t)}{dp}+\lambda E_{OV}\frac{t}{\tau}\{x(p,t)-x_e^*\}+\frac{KAZ}{L}\frac{t}{\tau}\left\{x(p,t)-\int_0^\infty x(p,q)\frac{q}{\tau}f(q)dq\right\}\right]dt=0 \quad . \tag{A1.2}$$

Further, the definition of mean residence time is

$$\tau=\int_0^\infty tf(t)dt \quad . \tag{A1.3}$$

The application of Eq. A1.3 transforms Eq. A1.2 as

$$\int_0^\infty f(t)\left[\frac{dx(p,t)}{dp}+\lambda E_{OV}\frac{t}{\tau}\{x(p,t)-x_e^*\}\right]dt=0 \quad . \tag{A1.4}$$

As $0<t<\infty$ and $f(t)\geq 0$ in the above equation, it is possible to write

$$\frac{dx(p,t)}{dp}+\lambda E_{OV}\frac{t}{\tau}\{x(p,t)-x_e^*\}=0 \quad . \tag{A1.5}$$

Eq. A1.5 is solved using method of separation of variables and subsequent application of the inlet boundary condition ($x|_{inlet}=x_{m-1}$) yields

$$\frac{x(p\,,t)-x_e^*}{x_{m-1}-x_e^*}=exp(-\lambda E_{OV}p\,t/\tau) \quad . \tag{A1.6}$$

The liquid-side Murphree tray efficiency is

$$E_{ML}=\frac{x_m-x_{m-1}}{x_m^*-x_{m-1}} \quad . \tag{A1.7}$$

The average composition of liquid leaving the tray can be calculated from Eq. A1.6 as

$$x_m=\int_0^\infty x(1,t)f(t)dt=\ x_e^*+(x_{m-1}-x_e^*)\int_0^\infty exp(-\lambda E_{OV}\,t/\tau)\,f(t)dt \quad . \tag{A1.8}$$

The material balance over the whole tray (see Fig. A1) relates Eq. A1.7 and Eq. A1.8 through x_m^* as

$$L(x_m-x_{m-1})=V(y_{in}-y_m)=mV(x_e^*-x_m^*) \quad . \tag{A1.9}$$

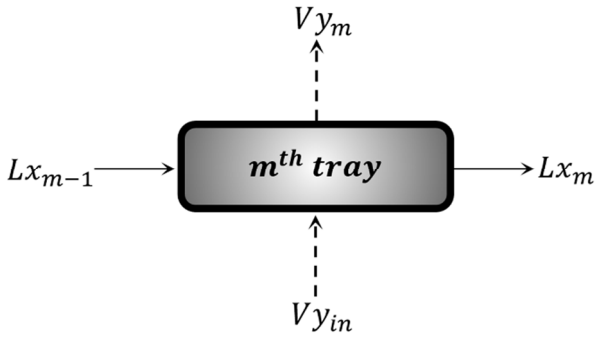

Fig. A1. Material balance over the whole tray.

Finally, the liquid-side tray efficiency is obtained using Eq. A1.7 to Eq. A1.9 as

$$E_{ML}=\frac{1-\int_0^\infty exp(-\lambda E_{OV}\,t/\tau)\,.\,f(t)dt}{1-\frac{1}{\lambda}\left\{1-\int_0^\infty exp(-\lambda E_{OV}\,t/\tau)\,.\,f(t)dt\right\}} \quad . \tag{A1.10}$$

Following similar procedure, the vapor-side tray efficiency can be acquired as

$$E_{MV} = \frac{1 - \int_0^\infty exp(-\lambda E_{OV}\, t/\tau)\,.\,f(t)dt}{\lambda \int_0^\infty exp(-\lambda E_{OV}\, t/\tau)\,.\,f(t)dt} \quad . \tag{6}$$

Appendix B: Mathematical validation of the RRTD model

B.1 Plug flow of liquid with any distribution of vapor flow over the tray

The tray is partitioned into n compartments with arbitrary distribution of area fraction and vapor allocation index as described in Eq. 9 to Eq. 11. During plug flow of liquid, the Murphree efficiency of the i^{th} compartment according to Lewis' Case I[19] is

$$\frac{E_{MV,i}}{E_{OV}} = \frac{e^{\lambda_i E_{OV}} - 1}{\lambda_i E_{OV}} = \frac{e^{a_i d_i \mu} - 1}{a_i d_i \mu} \quad . \tag{B1.1}$$

Substituting Eq. B1.1 in the RRTD model (i.e. Eq. 20) for $i = 1, 2, \dots n$ results in

$$\frac{E_{MV}^{+}}{E_{OV}} = \frac{e^{\mu} - 1}{\mu} \quad , \tag{B1.2}$$

which is Lewis' Case I for the tray itself. Since arbitrary distribution of the area fraction and the allocation index are considered here, Eq. B1.2 remains valid for uniform as well as non-uniform vapor flow through the tray. This equation also holds for non-uniform distribution of the area fraction among compartments.

B.2 Perfectly mixed pools of liquid during uniform vapor distribution over the tray

In the literature, the mixed pool model[21] has been formulated by considering identical pools of perfectly mixed liquid along the flow path on a tray. Further, uniform flow of vapor through these pools has been considered in this model, which yields

$$a_i = \frac{1}{n} \quad , \tag{B2.1}$$

$$d_i = 1 \quad \text{and} \tag{B2.2}$$

$$\frac{E_{MV,i}}{E_{OV}} = 1 \quad . \tag{B2.3}$$

Using Eq. B2.1 to Eq. B2.3 in Eq. 20 leads to

$$\frac{E_{MV}^{+}}{E_{OV}} = \frac{1}{\mu}\left\{\left(1+\frac{\mu}{n}\right)^{n} - 1\right\} \quad , \tag{B2.4}$$

which is the mixed pool model itself.

Appendix C: Deconvolution algorithm

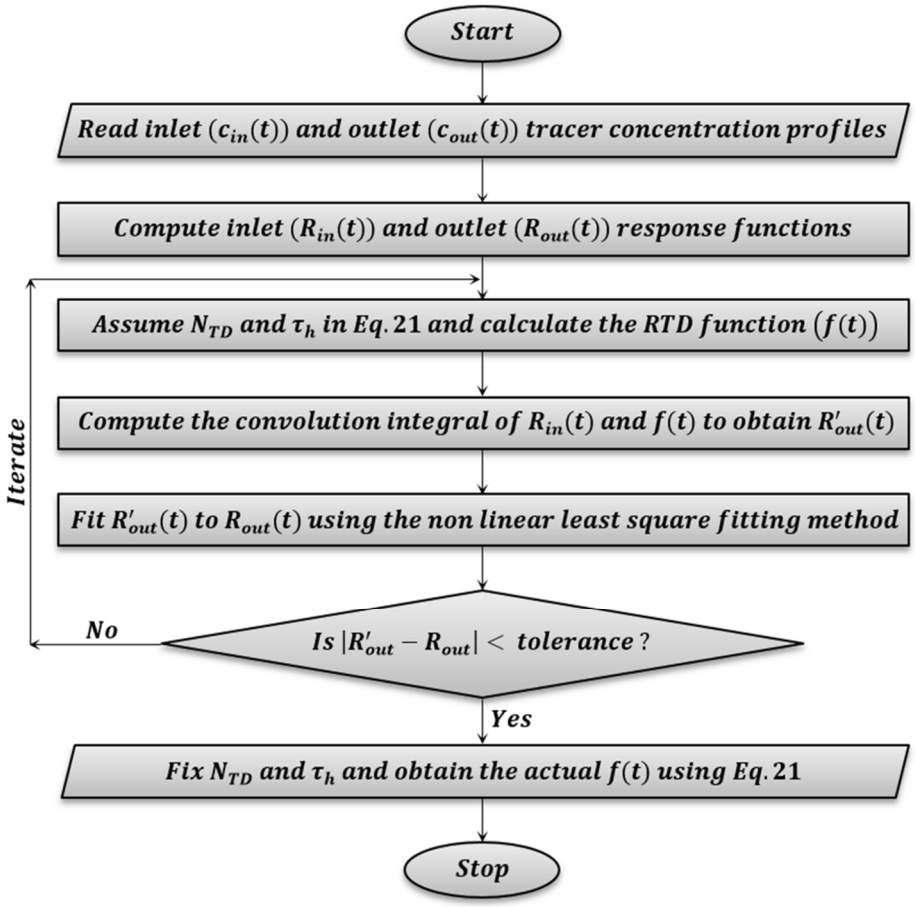

Fig. A2. Flowchart for obtaining the RTD function through model fitting (here, $R(t) = c(t)/\int_0^\infty c(t)\,dt$, and the terms 'inlet' and 'outlet' refer to either tray or compartment boundaries).

Graphical Abstract